Available online at www.sciencedirect.com

ScienceDirect

International Journal of Solids and Structures 44 (2007) 8532–8555

INTERNATIONAL JOURNAL OF SOLIDS AND STRUCTURES

www.elsevier.com/locate/ijsolstr

A numerical and experimental investigation into residual stress in thermally sprayed coatings

A.M. Kamara, K. Davey *

School of Mechanical, Aerospace and Civil Engineering, University of Manchester, United Kingdom

Received 16 November 2006; received in revised form 12 June 2007
Available online 20 August 2007

Abstract

This paper is concerned with an investigation into the thermal spray process and is particularly concerned with the residual stresses that arise when a steel-alloy coating is sprayed onto a copper-alloy substrate. This material combination was used recently to enhance the thermal and mechanical efficiency of the pressure die casting process. A difficulty with the spraying of steel on copper is the attainment of appreciable thickness of the coating due to debonding during the thermal spraying process. Prominent among possible causes of debonding is residual stress, which is the focus of the research presented in the paper. An investigation into the thermal spray process is performed using experimentation, simplified numerical modelling and finite element modelling. The development of residual stress for a range of process parameters, i.e. deposited layer thickness, interval of layer deposition and the number of layers in a coating (i.e. block deposition versus multilayer deposition for a desired coating thickness) is recorded. The results from the three investigation methods agreeably indicate a progressive change in average interfacial residual stress from compressive towards tensile with increase in thickness of deposited layer; and a tensile interfacial stress in a two-layer coating, which increases with increase in interval of deposition between the two layers. On the whole, the observations from the results suggest an increase in potential for coating debonding with increase in both deposited layer thickness and layer deposition interval. The results further suggest higher potential for coating debonding with block deposition compared to multilayer deposition for a desired coating thickness.

Keywords: Thermal spraying; Residual stress

1. Introduction

Thermal spray technology has become an important part of modern industry for the provision of coatings that offer customised surface properties for a variety of industrial applications. The technology, which has proved useful and cost effective, basically involves coating of a component referred to as the substrate with a molten or semi-molten material possessing good physical properties. The coating material, upon solidification enhances the properties of the base metals of the substrate and increases its service life and operational efficiency. This was demonstrated in the work of (Clarke et al., 2006), which among other aspects investigated

* Corresponding author. Tel.: +44 0 161 306 3834.
E-mail address: keith.davey@manchester.ac.uk (K. Davey).

0020-7683/$ - see front matter
doi:10.1016/j.ijsolstr.2007.06.031

the feasibility of using copper dies in pressure die casting processes. In that work the thermal spray technology was used in the deposition of chrome-steel coating layers on the cavity surface of a copper die for protection against abrasive wear and thermal shock.

Of fundamental importance to a coating is its bond strength with the substrate. This takes precedent because other performance characteristic such as corrosion resistance, wear resistance etc. cannot be realised without effective bonding. The mechanisms at play, at the coating-substrate interface, as well as between the particles making up the coating is an area that in many cases is still subject to speculation (Araujo et al., 2005). Also, the deterioration in bond strength, particularly with thick coatings, is of concern specifically with regard to premature debonding, which is a unique feature with such coatings. A credible hypothesis to explain the behaviour with thicker coatings is that coating defects and residual stress contribute to reduce bond strength, which in most cases can lead to failure during operation.

Efforts to address the wide range of effects from residual stress in thermally sprayed coatings have led to a multitude of research investigations (Kuroda and Clyne, 1991; Clyne and Gill, 1996; Tsui and Clyne, 1997a,b; Kesler et al., 1998; Lugscheider and Nickel, 2003 and Totemeire and Wright, 2006). Owing to the complex nature of the thermal spray process, the cooling method of a sprayed coating, and its associated material behaviour, it is difficult to accurately represent all the mechanisms involved when modelling residual stress. Various investigations have therefore made use of various assumptions. Prominent with analytical models is the assumption of elastic material behaviour. In this paper, simplified models are developed which incorporate plastic deformation, which predominantly takes place in the early stages of the spray deposition process.

During a thermal spray process, various factors contribute to residual stress generation; and these can be material or process dependent (Ahmed and Hadfield, 1997). This paper is focused on process-related factors such as coating deposition options during a thermal spray process; and specifically deposited layer thickness, interval of layer deposition and number of layers in a deposited coating. As a gateway to predicting the potential influence of these deposition options on coating performance, their effect on the nature of the residual stress and its change with increase in coating thickness are investigated using experimentation, a simplified numerical modelling method and the finite element method.

The investigation on deposited layer thickness considered four one-layer coatings of thicknesses of 0.1, 0.15, 0.2 and 0.3 mm, each solidifying on a 2 mm thick substrate. With regard to interval of layer deposition, three intervals of 30, 150 and 600 s were considered between the sequential depositions of two 0.1 mm thick coating layers to form a 0.2 mm thick coating system. For the investigation on number of layers in a coating, two coating specimens, each 0.2 mm thick were considered. One of these specimens has a single 0.2 mm thick layer, thereafter referred to as the one-layer coating and representing the effect of block deposition, while the other has two equal layers of 0.1 mm thick deposited sequentially, which is thereafter referred to as the two-layer coating and represents the effect of multi-layer deposition. In all cases, the substrate is at ambient initial conditions (assumed 20 °C) while a deposited coating layer is at the pouring temperature (assumed 1600 °C).

In the various investigations, the stress of interest is the stress in the direction of deposition (parallel to the interface) in the interior of the coating, which often forms the major component of stress compared to the interfacial shear and normal stresses. As mentioned in the literature (Withers and Bhadeshia, 2001; Borland, 1994; Noyan, 1992), depending on its magnitude of tensile stress in the coating, cracking can result, or alternatively with compressive or tensile stresses, bond failure can occur through interfacial shear. Potential influence of the selected coating deposition options on the latter effect is also investigated through a study of the average interfacial stress, σ_{inf} in a coated system. This bonding performance assessment parameter is defined as (Godoy et al., 2002):

$$\sigma_{\text{inf}} = \frac{\sigma_{\text{inf}}^{\text{c}} + \sigma_{\text{inf}}^{\text{s}}}{2} \tag{1}$$

where $\sigma_{\text{inf}}^{\text{c}}$ and $\sigma_{\text{inf}}^{\text{s}}$ are the interfacial in-plane residual stresses for the coating and the substrate, respectively.

2. Experimental investigation

Due to the influence of residual stress, certain thermally sprayed systems often adopt curvature whose direction and magnitude is dictated by the nature (i.e. direction) and the magnitude of the generated stress.

Monitored in this experimental investigation was the adopted curvature of copper substrates deposited with chrome steel coatings using the TAFA 8850MHU arc spray system. Being considered as a reliable residual stress depicting parameter, the adopted curvature is estimated for application into derived mathematical relations to calculate the generated residual stress in the thermally sprayed systems.

The use of curvature is one of the most well-established and common methods for predicting residual stress in coated systems; and has been extensively and successively used in a variety of coating residual stress related investigations (Larsson et al., 1996; Vijgoen and Dautzenberg, 1995; Gill and Clyne, 1994; Knight and Smith, 1993; Perry et al., 1996). Its popularity is based on its relatively low cost, readily availability of the measuring equipment and its simplicity for calculation. Monitoring the curvature of a substrate under successively deposited layers of coating can be achieved with a variety of methods, which depending on the resolution and range of measuring instruments include optical microscopy, laser scanning and strain gauges. In this work, use has been made of a Linear Variable Differential Transducer (LVDT); and the layout of the equipment used, the experimental and data acquisition procedures are discussed below.

2.1. Equipment layout and experimental procedure

As a first step in the coating process, the specimens were grit-blasted with alumina to clean off impurities. A bond coat of aluminium bronze (Cu 92.5, Al 7.0, Fe 0.5) was then applied onto the blasted surface prior to the application of the top-coat of chrome steel (Si 1.6, Cr 29.0, Mn 1.65, B 3.75, Fe 64). In practice this coating is much thinner than the top-coat and is similar, in this research, to the substrate material, chrome copper (Cu 99.1, Fe 0.01, Cr 0.60, Si 0.10, Mn 0.05) in terms of both being copper-based alloys. It was therefore assumed to be integrated within the thickness of the substrate for analysis purposes. To justify this assumption the bond-coat was sprayed on the entire length of a specimen at a fast speed, giving rise to negligible thicknesses in the range of 0.001–0.003 mm on the large number of specimens considered.

Monitoring of substrate curvature was commenced during the deposition of the top-coat, whose relatively thicker layers are viewed to have more impact on stress generation and curvature adoption. A schematic illustration of the main components in the experimental rig used to monitor the progressive changes in the substrate's deflection and curvature is shown in Fig. 1. For clarity, the figure is showing the rig in a 90° clockwise position relative to its orientation in a thermal spray process. Constituents of the rig include a strip shaped copper substrate (i.e. the specimen) of dimensions $2 \times 15 \times 120$ mm, which is attached to a pair of knife-edges by the pair of springs of negligible stiffness. The pair of control posts, which are positioned by the horizontal sides of the specimen, are meant to reduce or possibly overcome any vertical movement from it during spraying. The knife-edges are made from asbestos, a thermal insulating material specifically chosen to ensure no thermal expansion effect from them during spraying. The span, ℓ of the copper between the knife-edges is 80 mm. This is the effective length on which the coating is deposited during a spraying process. The extending 20 mm lengths of copper beyond each knife-edge, which are referred to as the ineffective lengths are prevented from contacting any sprayed coating by overhanging metallic flanges as shown in the figure.

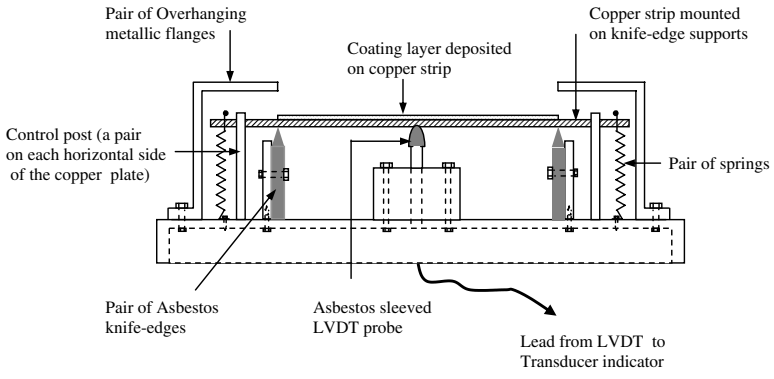

Fig. 1. A schematic illustration of the main components constituted in the experimental rig for coated substrate deflection measurement.

The LVDT, as shown also in Fig. 1 is positioned on the specimen such that its probe centrally contacts the back of the substrate. Similar to the knife-edges, the probe is sleeved with the asbestos material to prevent it from any thermal expansion effect that may arise from the temperature changes on the substrate due to the sprayed coating. With the attachment of the LVDT onto the appropriately mounted specimen on the rig, the rig is entered into the booth for spraying. The LVDT records the periodic central deflection of the substrate during the deposition of the coating layers and their subsequent cooling. The recording is affected by the connection of the transducer to a conditioning unit, which provides the energisation for data acquisition via an analogue variable voltage output.

For the 1.6 mm diameter feed wire of chrome steel (Si 1.6, Cr 29.0, Mn 1.65, B 3.75, Fe 64), the coating was sprayed at the rate of 3.64 kg/hr/100 A under recommended operating conditions of 200 A and 34 V. It is also worth mentioning at this point that the spraying process was carried out manually and despite the modifications carried out on the spray booth by introducing guard bars to control the spray distance to a recommended value of approximately 130 mm, the manual means of spraying resulted in other spraying conditions, particularly the deposited layer thickness and the spraying speed uncontrollable. It was therefore difficult to achieve a desired thickness of coating layer in a spray pass. To achieve the layers of thicknesses of 0.1, 0.15, 0.2 and 0.3 mm, which were used to investigate the effect of layer thickness on residual stress, several substrates with bond-coat thickness of 0.001 mm were considered. The initial thickness, h_s of each substrate was measured with Vernier callipers. Single coating layers were then randomly deposited on the substrates with the deflection history of each recorded during coating deposition and cooling down. For each sprayed substrate, the final thicknesses of the substrate/layer couple, h_{s_f} was also measured and the deposited layer thickness, h_ℓ obtained as $h_\ell = h_{s_f} - h_s$.

From the deposited layers, no layer thickness of 0.3 mm was achievable since all deposited layers of about that thickness were found to debond. This effect was attributed to either residual stress or other coating defective inclusions. However, layers with thicknesses approximate to 0.1, 0.15 and 0.2 mm, respectively, were achievable and for each of these layer thicknesses, four coated specimens were considered. The average periodic deflection of the specimens for each layer thickness was calculated. Over a period of 600 s, which was considered adequate for each deposited layer to have cooled down to approximately room temperature, these average deflection histories and the corresponding error bands for the specimens of the three achievable layer thicknesses are as shown in the plots in Fig. 2. For an average central deflection, δ, the corresponding curvature, κ is approximated as $\kappa = 8\delta/\ell^2$. At 600 s, the resulting average interfacial residual stress in the respective one-layer coating systems is obtained by applying the respective curvatures into a combination of Eq. (1) and Eqs. (A2), (A3) and (A4) in Appendix A. A plot of the variation of this stress with deposited layer thickness is shown in Fig. 3.

For the experimental investigation on the effect of layer deposition interval, 30, 150 and 600 s were the respective intervals considered between the depositions of two 0.1 mm coating layers. Due to limitation in the measuring equipment, the concern in this investigation was to achieve a final coating thickness of 0.2 mm from two deposited layers for each interval; and irrespective of the high level of uncertainty, the individual thicknesses of the deposited layers were assumed to be equal.

For each deposition interval, several substrates were similarly considered and the initial thickness for each substrate was measured prior to spraying. The two layers of coating were then deposited with the required deposition interval between them being monitored by the human controller of the spray gun using a stopclock. Throughout the spraying and the subsequent cooling of the layers over a period of 1200 s the deflection history of each substrate was recorded. After this period the thicknesses of the coated substrates were remeasured to deduce for each substrate the coating thickness obtained from the two deposited layers. For each of the deposition intervals four specimens of approximate two-layered coating thickness of 0.2 mm were considered; and as in the previous investigation, the average periodic deflection of the specimens for each interval was estimated. Over the considered period of 1200 s these average deflection histories and the corresponding error bands for the three deposition intervals are as shown in Fig. 4. Applying the corresponding curvature values at the end of the 1200 s into a combination of Eq. (1) and Eqs. (A7), (A8) and (A9) in Appendix A gives the corresponding values of the average interfacial residual stress in the respective two-layer coatings formed from the different deposition intervals. A plot of the variation of this stress with interval of layer deposition is presented in Fig. 5.

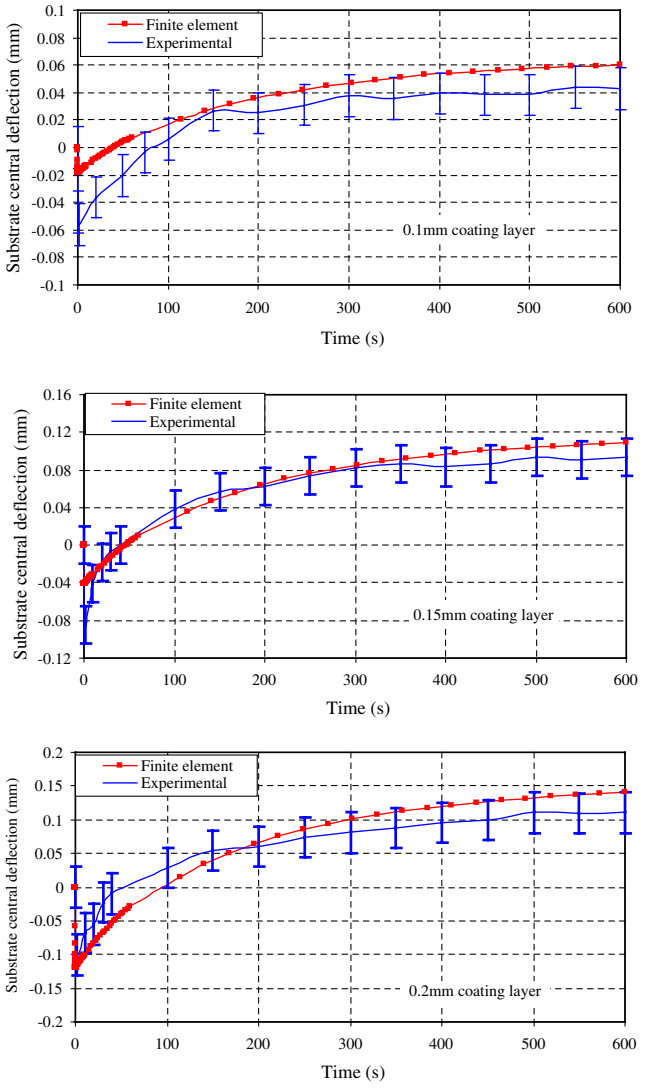

Fig. 2. Experimental results for the central deflection histories of the substrates of the 0.1, 0.15 and 0.2 mm coating layers over a cooling period of 600 s for each layer. Included are the corresponding results from the finite element modelling for comparison.

With regard to the experimental investigation on the effect of number of layers in a coating, Fig. 6 shows the average interfacial residual stress for the one-layer and the two-layer coating systems as extracted from the result of the 0.2 mm coating system in Fig. 2 and that of the two 0.1 mm coatings deposited at the interval of 600 s in Fig. 4. The choice of this interval's result for the two-layer coating is based on the worst stress situation portrayed to be obtained with it compared to those from the 30 and 150 s intervals. As can be seen in Fig. 6, the experimental average interfacial stresses in the two systems have opposite signs.

3. Simplified numerical modelling

In order to highlight the important physics involved in the prediction of stresses in deposited layers, simplified numerical models are investigated. Models involving non-linear ordinary differential equations are considered as these are easily solved using readily available solvers. To arrive at these types of equations certain assumptions have to be made. In particular, it is assumed here that a deposited coating layer undergoes two cooling phases (i.e. the quenching phase and the final cooling phase) during its cooling process. Also assumed

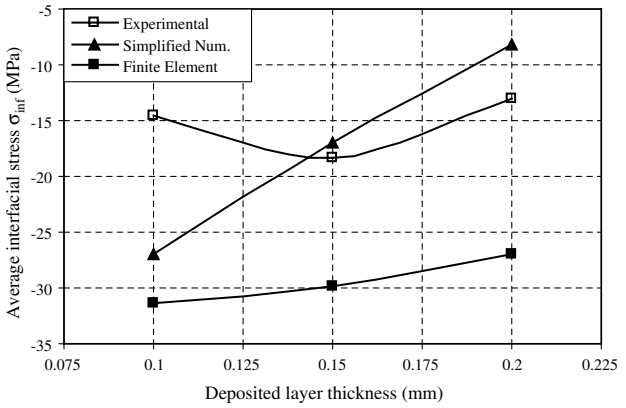

Fig. 3. Variation of average interfacial residual stress with deposited layer thickness.

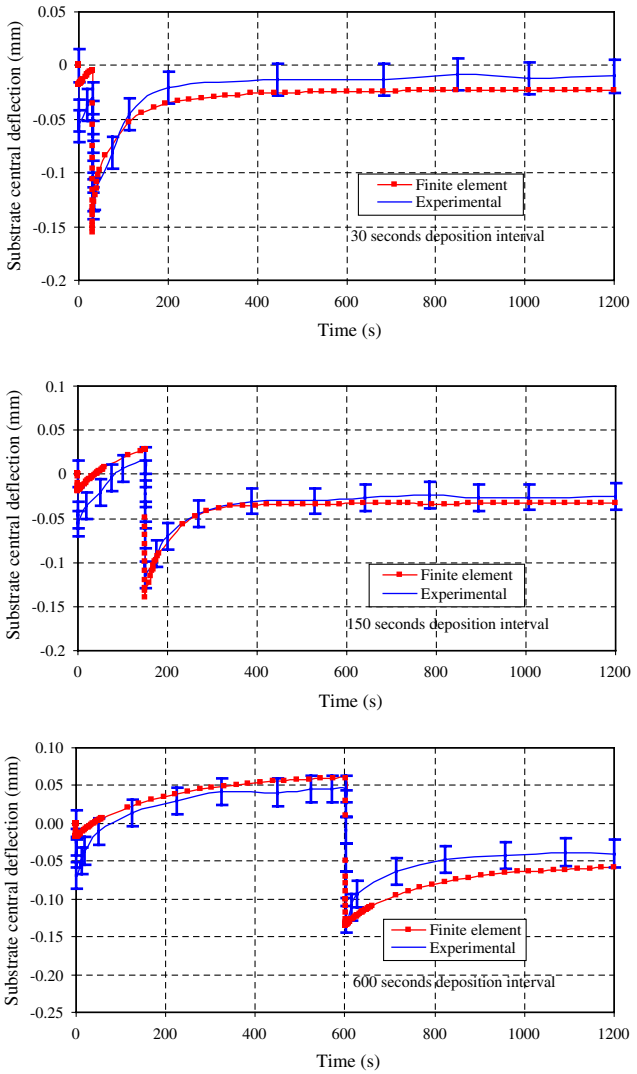

Fig. 4. Experimental results for the central deflection histories of the substrates for the two 0.1 mm coating layers deposited sequentially at 30, 150 and 600 s deposition intervals, respectively. Included are the corresponding results from the finite element modelling for comparison.

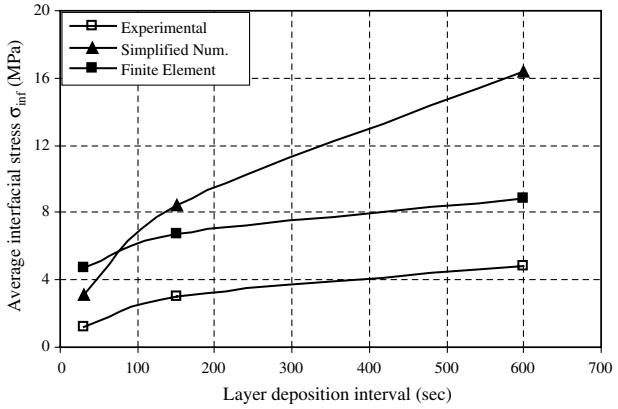

Fig. 5. Variation of average interfacial stress with interval of layer deposition.

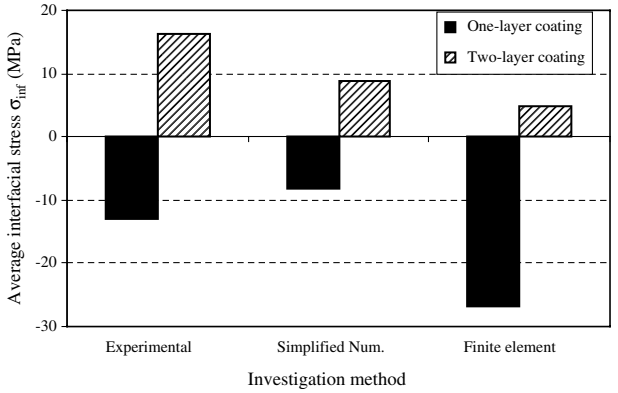

Fig. 6. Comparison of the average interfacial stress in the One-layer and the Two-layer coating systems.

is that the layer yields during its quenching phase according to von Mises yield criterion and behaves elastically during the final cooling phase. Furthermore, plane strain and plane stress formulation for the layer and the substrate are assumed respectively.

The stress in a layer is determined through a numerical approach involving two sequential analyses. This is such that the first analysis uses the stress-free condition of the layer at the pouring temperature, T_p, as an initial condition to determine the stress at the end of the quenching phase (i.e. at the temperature, T_q). In the subsequent analysis, the stress at the end of the quenching phase is used as initial condition to determine the stress at the end of the final cooling phase (i.e. at the temperature, T_f), which ultimately defines the residual stress. As with the experimental investigations, use is also made of a one-layer and a two-layer system in this investigation method.

In the analysis that follows, the subscripts, (x), (y) and (z), respectively, denote the global x, y and z directions while ℓ and s denote parameters relating to the layer and the substrate, respectively. The superscripts (q) and (f) are used to identify parameters referring to the quenching phase and the final cooling phase of a layer, respectively.

3.1. Stress in a one-layer coating/substrate system

A 2-D configuration of this system is as shown in Fig. 7, in which the assumed molten coating layer of thickness h_ℓ is shown to be deposited onto the substrate of thickness h_s, which is of width b, measured in the z-direction. During the quenching phase, which is assumed to be influenced by the interfacial surface of

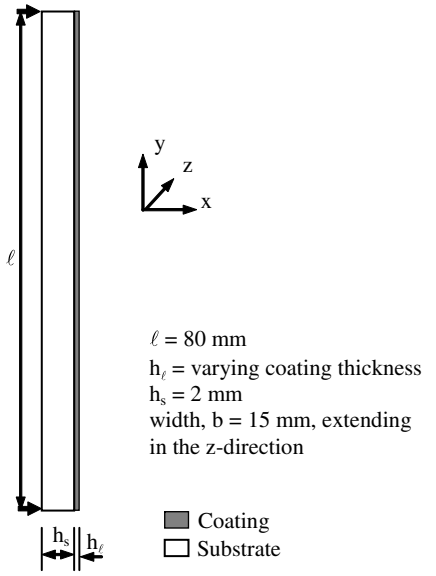

Fig. 7. A schematic illustration of a one-layer coating/substrate system as supported on knife-edges during a spray process.

the substrate, the layer experiences an incremental stress. This is a consequence of an incremental strain, which due to the thin nature of the layer is assumed uniform. Assuming also that the total effect of this incremental strain is a superposition of plastic, elastic and thermal components implies

$$\mathrm{d}\varepsilon^{\mathrm{tot(q)}}_{\ell(x)} = \mathrm{d}\varepsilon^{\mathrm{e(q)}}_{\ell(x)} + \mathrm{d}\varepsilon^{\mathrm{p(q)}}_{\ell(x)} + \mathrm{d}\varepsilon^{\mathrm{th(q)}}_{\ell(x)} \tag{2}$$

$$\mathrm{d}\varepsilon^{\mathrm{tot(q)}}_{\ell(y)} = \mathrm{d}\varepsilon^{\mathrm{e(q)}}_{\ell(y)} + \mathrm{d}\varepsilon^{\mathrm{p(q)}}_{\ell(y)} + \mathrm{d}\varepsilon^{\mathrm{th(q)}}_{\ell(y)} \tag{3}$$

where the superscripts, tot, e, p and th identify the total, elastic, plastic and thermal components of strain, respectively.

Focus here is on stress and strains associated with the x–y plane with stress in the y-direction being particularly significant. Following the assumption that $\sigma^{(\mathrm{q})}_{\ell(z)} \approx 0$, Eqs. (2) and (3) can then be rewritten as

$$\mathrm{d}\varepsilon^{\mathrm{tot(q)}}_{\ell(x)} = \frac{1}{E_\ell}\left(\mathrm{d}\sigma^{(\mathrm{q})}_{\ell(x)} - \nu_\ell \mathrm{d}\sigma^{(\mathrm{q})}_{\ell(y)}\right) + \sigma'^{(\mathrm{q})}_{\ell(x)}\mathrm{d}\lambda^{(\mathrm{q})} + \alpha_\ell\,\mathrm{d}T_\ell \tag{4}$$

$$\mathrm{d}\varepsilon^{\mathrm{tot(q)}}_{\ell(y)} = \frac{1}{E_\ell}\left(\mathrm{d}\sigma^{(\mathrm{q})}_{\ell(y)} - \nu_\ell \mathrm{d}\sigma^{(\mathrm{q})}_{\ell(x)}\right) + \sigma'^{(\mathrm{q})}_{\ell(y)}\mathrm{d}\lambda^{(\mathrm{q})} + \alpha_\ell\,\mathrm{d}T_\ell \tag{5}$$

where E, ν, σ' and $\mathrm{d}\lambda$ are Young's modulus, Poisson's ratio, deviatoric stress and differential of plastic modulus, respectively. The approximation $\sigma^{(\mathrm{q})}_{\ell(z)} \approx 0$ combined with the plane-strain condition $\mathrm{d}\varepsilon^{\mathrm{tot(q)}}_{\ell(z)} \approx 0$ invokes a balance between differential, elastic, thermal and plastic strains in the z-direction. The mean stress, $\sigma_{\mathrm{m}} = (\sigma_{\ell(y)} + \sigma_{\ell(x)})/3$ and substituting the resulting values for the deviatoric stresses, $\sigma'_{\ell(x)}$ and $\sigma'_{\ell(y)}$ into Eqs. (4) and (5), respectively, gives

$$\mathrm{d}\varepsilon^{\mathrm{tot(q)}}_{\ell(x)} = \frac{1}{E_\ell}\left(\mathrm{d}\sigma^{(\mathrm{q})}_{\ell(x)} - \nu_\ell \mathrm{d}\sigma^{(\mathrm{q})}_{\ell(y)}\right) + \left(\frac{2\sigma^{(\mathrm{q})}_{\ell(x)} - \sigma^{(\mathrm{q})}_{\ell(y)}}{3}\right)\mathrm{d}\lambda^{(\mathrm{q})} + \alpha_\ell\,\mathrm{d}T_\ell \tag{6}$$

$$\mathrm{d}\varepsilon^{\mathrm{tot(q)}}_{\ell(y)} = \frac{1}{E_\ell}\left(\mathrm{d}\sigma^{(\mathrm{q})}_{\ell(y)} - \nu_\ell \mathrm{d}\sigma^{(\mathrm{q})}_{\ell(x)}\right) + \left(\frac{2\sigma^{(\mathrm{q})}_{\ell(y)} - \sigma^{(\mathrm{q})}_{\ell(x)}}{3}\right)\mathrm{d}\lambda^{(\mathrm{q})} + \alpha_\ell\,\mathrm{d}T_\ell \tag{7}$$

The substrate, which is generally assumed to behave elastically and in plane stress, is assumed to act rigidly in the x-direction during the quenching phase, as it is subject to low levels of stress arising from the solidification of a comparatively soft layer. This implies

$$\mathrm{d}\varepsilon_{\mathrm{s}(x)}^{\mathrm{tot(q)}} = 0 \tag{8}$$

In addition, owing to the very short duration for the quenching phase, the interaction of the substrate with the layer is assumed to be felt only at the interfacial surface of the substrate with no deformation in the body of the substrate. It should be recognised that the layer is initially comparatively soft compared to the substrate and the region of the substrate close to the interface will strain, although principally as a consequence of thermal expansion. In the y-direction the total strain differential at the interfacial surface of the substrate is therefore assumed to be

$$\mathrm{d}\varepsilon_{\mathrm{s}(y)}^{\mathrm{tot(q)}} = \mathrm{d}\varepsilon_{\mathrm{s}(y)}^{\mathrm{th(q)}} = \alpha_{\mathrm{s}}\,\mathrm{d}T_{\mathrm{s}} \tag{9}$$

For compatibility of the layer/substrate system, the differential strains of the two domains at the interfacial surfaces are equal, i.e. $\mathrm{d}\varepsilon_{\ell(x)}^{\mathrm{tot(q)}} = \mathrm{d}\varepsilon_{\mathrm{s}(x)}^{\mathrm{th(q)}}$ and $\mathrm{d}\varepsilon_{\ell(y)}^{\mathrm{tot(q)}} = \mathrm{d}\varepsilon_{\mathrm{s}(y)}^{\mathrm{th(q)}}$.

Combine Eqs. (6) and (8); and Eqs. (7) and (9), and on simplification gives

$$\dot{\sigma}_{\ell(x)}^{(\mathrm{q})} - \nu_{\ell}\dot{\sigma}_{\ell(y)}^{(\mathrm{q})} + E_{\ell}\left(\frac{2\sigma_{\ell(x)}^{(\mathrm{q})} - \sigma_{\ell(y)}^{(\mathrm{q})}}{3}\right)\dot{\lambda}^{(\mathrm{q})} = -E_{\ell}\alpha_{\ell} \tag{10}$$

$$\dot{\sigma}_{\ell(y)}^{(\mathrm{q})} - \nu_{\ell}\dot{\sigma}_{\ell(x)}^{(\mathrm{q})} + E_{\ell}\left(\frac{2\sigma_{\ell(y)}^{(\mathrm{q})} - \sigma_{\ell(x)}^{(\mathrm{q})}}{3}\right)\dot{\lambda}^{(\mathrm{q})} = E_{\ell}\left(\alpha_{\mathrm{s}}\frac{\mathrm{d}T_{\mathrm{s}}}{\mathrm{d}T_{\ell}} - \alpha_{\ell}\right) \tag{11}$$

where $\dot{\sigma}$ and $\dot{\lambda}$ are first derivatives with respect to the layer temperature T_{ℓ}.

Also, during the quenching phase, the changes in the temperature, T_{ℓ} of the layer has a corresponding impact on the temperature, T_{s} of the substrate. At the interfacial surface, this is such that initially $T_{\mathrm{s}} = T_{\mathrm{r}}$ and $T_{\ell} = T_{\mathrm{p}}$ and at the end of the quenching phase $T_{\mathrm{s}} = T_{\ell} = T_{\mathrm{q}}$, where T_{r} is room temperature. Assuming linear thermal behaviour between the interfacial surfaces, a relation for the interfacial temperature of the substrate is deduced as $T_{\mathrm{s}} = [T_{\mathrm{r}}(T_{\ell} - T_{\mathrm{q}}) - T_{\mathrm{q}}(T_{\ell} - T_{\mathrm{p}})]/(T_{\mathrm{p}} - T_{\mathrm{q}})$ and from which $\mathrm{d}T_{\mathrm{s}}/\mathrm{d}T_{\ell} = (T_{\mathrm{r}} - T_{\mathrm{q}})/(T_{\mathrm{p}} - T_{\mathrm{q}})$ is for substitution into Eq. (11).

Considering also the assumption that a deposited layer yields during its quenching process, and that such yielding obeys the von Mises criterion implies $\left[\sigma_{\ell(y)}^{(\mathrm{q})}\right]^2 - \sigma_{\ell(y)}^{(\mathrm{q})}\sigma_{\ell(x)}^{(\mathrm{q})} + \left[\sigma_{\ell(x)}^{(\mathrm{q})}\right]^2 = [Y]^2$, which can be expressed in the form

$$\left(2\sigma_{\ell(y)}^{(\mathrm{q})} - \sigma_{\ell(x)}^{(\mathrm{q})}\right)\dot{\sigma}_{\ell(y)} + \left(2\sigma_{\ell(x)}^{(\mathrm{q})} - \sigma_{\ell(y)}^{(\mathrm{q})}\right)\dot{\sigma}_{\ell(x)}^{(\mathrm{q})} = 2Y\dot{Y} \tag{12}$$

where $Y = Y(T_{\ell})$, is the temperature-dependent yield stress of a layer and $\dot{Y}$ is its first derivative with respect to T_{ℓ}.

In the absence of material properties for chrome steel (Si 1.6, Cr 29.0, Mn 1.65, B 3.75, Fe 64.0), those for 304L stainless steel, which are readily available were assumed for the coating. As adopted from Ortega et al. (1998), the curve, $Y(T_{\ell})$ in Fig. 8 depicts the yield stress variation with temperature for this material and is hereafter assumed as a pattern for yielding-related stress, $\sigma_{\ell}(T_{\ell})$ in any deposited layer of coating. In terms of its stress-free temperature, which is the melting temperature, T_{m}, room temperature, T_{r} and its yield stress at room temperature Y_{r}, (which is the maximum attainable stress by the coating during yielding), the stress, $\sigma_{\ell}(T_{\ell})$, is approximated to have a relation of the form

$$\sigma_{\ell}(T_{\ell}) = Y(T_{\ell}) = Y_{\mathrm{r}}\left(\frac{T_{\ell} - T_{\mathrm{m}}}{T_{\mathrm{r}} - T_{\mathrm{m}}}\right)^{\gamma} \tag{13}$$

where γ is an index, which was determined through curve-fitting; and its value is that on the curve, $\sigma_{\ell}(T_{\ell})$, which provides the best fit to the curve, $Y(T_{\ell})$. Curves for $\gamma < 1$, $\gamma = 1$ and $\gamma > 1$ were examined. It is evident in Fig. 8 that the curve for $\gamma = 2$, not only proves to have the best fit but also has zero gradient at T_{m} as required.

The stress state of the layer at the end of its quenching phase is obtained from a solution of the first-order initial value ordinary differential equations defined by Eqs. (10)–(12). Defining $\beta_0 = \sigma_{\ell(x)}^{(\mathrm{q})}$, $\beta_1 = \sigma_{\ell(y)}^{(\mathrm{q})}$ and $\beta_2 = E_{\ell}\lambda^{(\mathrm{q})}$, these equation are written in the matrix form as

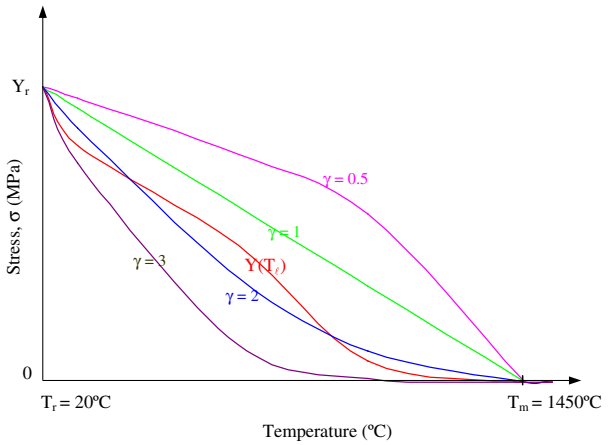

Fig. 8. Increasing yield stress from zero at $T \geqslant T_m$ to Y_r at $T = T_r$ during the cooling down of a deposited molten layer of coating.

$$D(T,\beta) = \begin{pmatrix} \dot{\beta}_1 \\ \dot{\beta}_2 \\ \dot{\beta}_3 \end{pmatrix} = \begin{bmatrix} 1 & -\nu_\ell & \frac{(2\beta_0-\beta_1)}{3Y(T)} \\ -\nu_\ell & 1 & \frac{(2\beta_1-\beta_0)}{3Y(T)} \\ \frac{(2\beta_0-\beta_1)}{Y(T)} & \frac{(2\beta_1-\beta_0)}{Y(T)} & 0 \end{bmatrix}^{-1} \begin{bmatrix} -E_\ell\alpha_\ell \\ E_\ell\left(\alpha_s\left(\frac{T_r-T_q}{T_p-T_q}\right)-\alpha_\ell\right) \\ 2\dot{Y} \end{bmatrix} \tag{14}$$

where $D(T,\beta)$ is a function which gives the vector of the derivatives, $\dot{\beta}_0$, $\dot{\beta}_1$ and $\dot{\beta}_2$ at any solution point (T,β). It is worth mentioning here that β_i, $i = 0, 1, 2$, are defined, and the equations arranged in (14), to ensure coefficients in the matrix are of similar magnitude. Problems did result with other choices arising for the poor condition of the matrix in Eq. (14) and the inability of the numerical solver to deal with this. Also, in order to avoid the problem of division by zero in Eq. (21) at $T = T_p = T_m$, as a result of $Y(T_m) = 0$, the solution procedure is initialised at $T_m - 1$, i.e. one degree below the solidification temperature of the layer material. At this temperature the initial conditions are $\beta_0(T_m - 1) = \beta_1(T_m - 1) = Y(T_m - 1)$ and $\beta_2(T_m - 1) = 0$. For the cooling of a layer from the deposition temperature, $T_p = T_m - 1$ to the quenching temperature, T_q, the adaptive Runge-Kutta function found in the MathCad software (see Appendix B for details) was used to obtain a solution for β_0, β_1 and β_2 at the solution points (T,β).

For the final cooling phase, which starts from the quenching temperature, T_q to some final cooled down temperature, T_f, the initial condition of the layer is that defined by its stress condition, $\beta_0(T_q)$, $\beta_1(T_q)$ and $\beta_2(T_q)$ at the end of the quenching phase. Also, the assumption that the layer behaves elastically during this cooling phase makes Eq. (12) invalid while the absence of yielding reduces Eq. (10) to

$$\dot{\sigma}^{(f)}_{\ell(x)} - \nu_\ell \dot{\sigma}^{(f)}_{\ell(y)} = -E_\ell\alpha_\ell \tag{15}$$

It should be appreciated also that during this cooling phase, the substrate temperature initially rises to unify with the entire system prior to final cooling. It is possible that further yielding occurs in the layer during this phase of temperature unification but this is assumed to be of minor significance and ignored in this analysis. Temperatures are assumed to be uniform following this unification and in the in-plane direction the total strain increment in the substrate is considered to be a combination of elastic and thermal components such that

$$\mathrm{d}\varepsilon^{\mathrm{tot(f)}}_{s(y)} = \mathrm{d}\varepsilon^{\mathrm{e(f)}}_{s(y)} + \mathrm{d}\varepsilon^{\mathrm{th(f)}}_{s(y)} \tag{16}$$

Note that at the interfacial surface of the substrate, the elastic strain differential, $\mathrm{d}\varepsilon^{\mathrm{e(f)}}_{s(y)}$, which is due to bending, is defined as $\mathrm{d}\varepsilon^{\mathrm{e(f)}}_{s(y)} = [(h_s/2) - w_N]\mathrm{d}\kappa$, where as defined in Eq. (A2) in Appendix A, w_N is the distance of the interfacial surface of the substrate from the neutral axis of the layer/substrate system and $\mathrm{d}\kappa$ is the differential change in curvature of the substrate, which as defined in Eq. (A4) in Appendix A as $\mathrm{d}\kappa = \phi\mathrm{d}\sigma^{(f)}_{\ell(y)}$, where the

value of the parameter ϕ, is deduced from this equation as $\phi = -6bh_\ell(h_s + h_\ell - 2w_N)/E_s(bh_s^3 + 12bh_s w_N^2)$. Substituting for $d\varepsilon^{e(f)}_{s(y)}$ into Eq. (16) gives

$$d\varepsilon^{tot(f)}_{s(y)} = \left(\frac{h_s}{2} - w_N\right)\phi\, d\sigma^{(f)}_{\ell(y)} + \alpha_s\, dT_\ell \tag{17}$$

In the y-direction the total differential strain in the layer during the final cooling phase is of the form of Eq. (6). Removal of the plastic terms from that equation to reflect elastic behaviour from the layer during this final cooling phase gives

$$d\varepsilon^{tot(f)}_{\ell(y)} = \frac{1}{E_\ell}\left(d\sigma^{(f)}_{\ell(y)} - \nu_\ell\, d\sigma^{(f)}_{\ell(x)}\right) + \alpha_\ell\, dT_\ell \tag{18}$$

For interfacial strain compatibility, $d\varepsilon^{tot(f)}_{\ell(y)} = d\varepsilon^{tot(f)}_{s(y)}$. Combining therefore Eqs. (17) and (18) gives

$$\left\{1 - \left(\frac{h_s}{2} - w_N\right)\phi E_\ell\right\}\dot{\beta}_1 - \nu_\ell\dot{\beta}_0 = E_\ell(\alpha_s - \alpha_\ell) \tag{19}$$

Eqs. (15) and (19), in which $\beta_0 = \sigma^{(f)}_{\ell(x)}$ and $\beta_1 = \sigma^{(f)}_{\ell(y)}$, form the set of the first-order initial value ordinary differential equations to be solved to obtain the stress condition in a layer at the end of the final cooling phase. The matrix form of these equations is

$$D(T,\beta) = \begin{pmatrix}\dot{\beta}_0\\ \dot{\beta}_1\end{pmatrix} = \begin{bmatrix}1 & -\nu\\ -\nu & \left\{1 - \left(\frac{h_s}{2} - w_N\right)\phi E_\ell\right\}\end{bmatrix}^{-1}\begin{bmatrix}-E_\ell\alpha_\ell\\ E_\ell(\alpha_s - \alpha_\ell)\end{bmatrix} \tag{20}$$

Similar to Eq. (14), this system is in a form that is readily solvable using the adaptive Runge-Kutta function. The solution function for this matrix contains T_q and T_f as initial and final temperatures, respectively; and the vector, $Y0$ of initial conditions holds the values $\beta_0(T_q)$, $\beta_1(T_q)$ and $\beta_2(T_q)$. From the resulting matrix of solution vectors for $\beta_0(T_\ell)$ and $\beta_1(T_\ell)$, the value, $\beta_1(T_f)$ represents the in-plane stress, $\sigma^{(f)}_{\ell(y)}$. This stress, which represents the change in stress in the layer from its initial stress-free state to its final cool down state defines the residual stress; and for convenience it is identified as $\Delta\sigma_\ell$.

The matrices in Eqs. (14) and (20), and their respective solution functions provide predictions for the residual stress in a one-layer system, but require information for the quenching temperature T_q of the layer and the temperature T_f to which it is finally cooled down over a given period of time. As estimated from the thermal results of the finite element modelling, T_q is throughout assumed as that temperature from which the layer commences continuous cooling while in contact with the substrate. As illustrated in Fig. 9, which shows the temperature history of the 0.1 mm coating and its substrate, estimated values for T_q and T_f are approximately 491 and 27 °C, respectively. From similar temperature histories for the 0.15 and 0.2 mm coating layers, the corresponding estimates for these temperatures are 496 and 31 °C, and 497 and 36 °C, respectively.

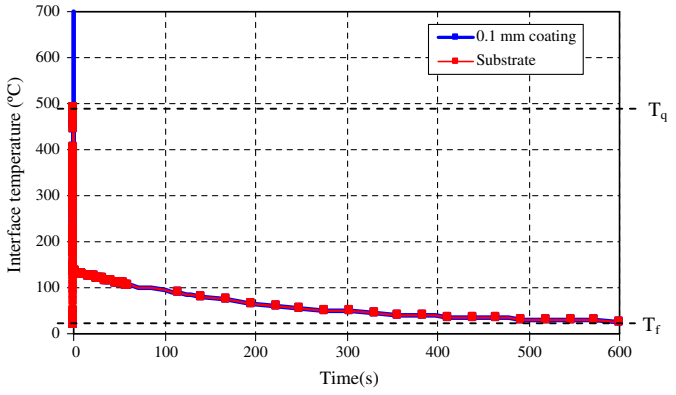

Fig. 9. Temperature history of the 0.1 mm coating and its substrate, depicting estimation of the temperatures, T_q and T_f for such one-layer coatings.

Respective applications of these values into the appropriate matrices or solution functions gives the respective values of the stress, $\Delta\sigma_\ell$, for the different coating layers. Applying the stress values into a combination of Eq. (1) and Eqs. (A2), (A3) and (A4) in Appendix A gives the corresponding values of the average interfacial stresss in the different one-layer coating/substrate systems. A plot of the variation of this stress with deposited layer thickness is superimposed in Fig. 3 for comparison with the corresponding plots from the other methods of investigation.

3.2. Stress in a two-layer coating/substrate system

This system has a similar layout to that shown in Fig. 7 but constituting two layers of coating, which are assumed to be of equal thickness, h_ℓ, and deposited sequentially onto the substrate. The notation, the first deposited layer is Layer 1 while the second is Layer 2, is maintained. The formation of this system is considered to be equivalent to the deposition of a second layer onto a one-layer system. The analysis of the residual stress in the two-layer system adopts the approach of superimposing the residual stress generated in the one-layer system (i.e. the composite of the substrate and Layer 1, which is hereafter called composite S1) to the incremental stress due to the deposition of Layer 2 onto that system. In addition to all previously used symbols, which bear their usual meanings, the superscript (r) is introduced to identify parameters referring the reheating phase of a previously deposited layer due to the effect of a currently deposited layer. Also introduced is the subscript, 2ℓ to denote parameters referring to the so-formed coating from the combination of Layers 1 and 2 while s1 is to parameters referring to composite S1. The sub-subscripts 1 and 2 on the subscript ℓ refer to Layers 1 and 2, respectively; and on all other parameters, these sub-subscripts denote effects from Layers 1 and 2, respectively, on those parameters.

Based on the above concept of formation for this system, Layer 2 is thus considered to be quenched by the interfacial surface of the underlying pre-stressed composite S1. This quenching, which gives rise to a stress increment in Layer 2 is a consequence of a strain increment, which is assumed to be uniform and constituting elastic, plastic and thermal components. Following a similar argument to that for the quenching of the layer by the substrate in the previous analysis for the one-layer system, Eqs. (6)–(8) are valid for the quenching of Layer 2 by the composite S1 in the formation of a two-layer system. To reflect the adopted notation in the analysis of the two-layer system, these equations take the respective forms

$$\mathrm{d}\varepsilon^{\mathrm{tot(q)}}_{\ell_2(x)} = \frac{1}{E_\ell}\left(\mathrm{d}\sigma^{(\mathrm{q})}_{\ell_2(x)} - \nu_\ell\,\mathrm{d}\sigma^{(\mathrm{q})}_{\ell_2(y)}\right) + \left(\frac{2\sigma^{(\mathrm{q})}_{\ell_2(x)} - \sigma^{(\mathrm{q})}_{\ell_2(y)}}{3}\right)\mathrm{d}\lambda^{(\mathrm{q})} + \alpha_\ell\,\mathrm{d}T_{\ell_2} \tag{21}$$

$$\mathrm{d}\varepsilon^{\mathrm{tot(q)}}_{\ell_2(y)} = \frac{1}{E_\ell}\left(\mathrm{d}\sigma^{(\mathrm{q})}_{\ell_2(y)} - \nu_\ell\,\mathrm{d}\sigma^{(\mathrm{q})}_{\ell_2(x)}\right) + \left(\frac{2\sigma^{(\mathrm{q})}_{\ell_2(y)} - \sigma^{(\mathrm{q})}_{\ell_2(x)}}{3}\right)\mathrm{d}\lambda^{(\mathrm{q})} + \alpha_\ell\,\mathrm{d}T_{\ell_2} \tag{22}$$

$$\mathrm{d}\varepsilon^{\mathrm{tot(q)}}_{\mathrm{s1}(x)} = 0 \tag{23}$$

Also, no elastic effects are assumed to be generated in the composite S1 due to the assumed localisation of the quenching phase. The total strain differential in the composite in the y-direction is hence assumed to be only due to thermal expansion. Moreover, since Layer 2 is deposited directly on the layer part of the composite where the thermal expansion coefficient is α_ℓ, this strain differential, $\mathrm{d}\varepsilon^{\mathrm{tot(q)}}_{\mathrm{s1}(y)}$, which is thus assumed to be dictated by that part of the composite takes the definition

$$\mathrm{d}\varepsilon^{\mathrm{tot(q)}}_{\mathrm{s1}(y)} = \mathrm{d}\varepsilon^{\mathrm{th(q)}}_{\mathrm{s1}(y)} = \alpha_\ell \mathrm{d}T_{\mathrm{s1}} \tag{24}$$

Strain compatibility condition in the system of Layer 2 and Composite S1 requires that the differential strains of the two domains at the interfacial surfaces are equal; this implies $\mathrm{d}\varepsilon^{\mathrm{tot(q)}}_{\ell_2(x)} = \mathrm{d}\varepsilon^{\mathrm{th(q)}}_{\mathrm{s1}(x)}$ and $\mathrm{d}\varepsilon^{\mathrm{tot(q)}}_{\ell_2(y)} = \mathrm{d}\varepsilon^{\mathrm{th(q)}}_{\mathrm{s1}(y)}$

Combining Eqs. (21) and (23); and Eqs. (22) and (24) gives

$$\dot{\sigma}^{(\mathrm{q})}_{\ell_2(x)} - \nu_\ell\dot{\sigma}^{(\mathrm{q})}_{\ell_2(y)} + E_\ell\left(\frac{2\sigma^{(\mathrm{q})}_{\ell_2(x)} - \sigma^{(\mathrm{q})}_{\ell_2(y)}}{3}\right)\dot{\lambda}^{(\mathrm{q})} = -E_\ell\alpha_\ell \tag{25}$$

$$\dot{\sigma}^{(q)}_{\ell_2(y)} - \nu_\ell \dot{\sigma}^{(q)}_{\ell_2(x)} + E_\ell \left(\frac{2\sigma^{(q)}_{\ell_2(y)} - \sigma^{(q)}_{\ell_2(x)}}{3} \right) \dot{\lambda}^{(q)} = E_\ell \alpha_\ell \left(\frac{dT_{s1}}{dT_{\ell_2}} - 1 \right) \tag{26}$$

where in this case, $\dot{\sigma}$ and $\dot{\lambda}$ are first derivatives with respect to the temperature, T_{ℓ_2}.

At the interfacial surfaces of Layer 2 and composite S1, the temperatures are such that initially $T_{s1} = T_i$ and $T_{\ell_2} = T_p$ and at the end of the quenching process $T_{s1} = T_{q_2}$ and $T_{\ell_2} = T_{q_2}$; and an assumed linear temperature for T_{s1} is of the form $T_{s1} = [T_i(T_{\ell_2} - T_{q_2}) - T_{q_2}(T_{\ell_2} - T_p)]/(T_p - T_{q_2})$. To be substituted into Eq. (26) is $dT_{s1}/dT_{\ell_2} = (T_i - T_{q_2})/(T_p - T_{q_2})$, where T_i is the equilibrium temperature of composite S1 at the deposition of Layer 2 and whose magnitude depends on the time interval that elapsed before the deposition of the latter.

The assumed yielding of Layer 2 during quenching makes Eq. (12) applicable and on differentiation with respect to T_{ℓ_2} gives

$$\left(2\sigma^{(q)}_{\ell_2(y)} - \sigma^{(q)}_{\ell_2(x)}\right)\dot{\sigma}_{\ell_2(y)} + \left(2\sigma^{(q)}_{\ell_2(x)} - \sigma^{(q)}_{\ell_2(y)}\right)\dot{\sigma}^{(q)}_{\ell_2(x)} = 2Y\dot{Y} \tag{27}$$

Eqs. (25)–(27) are the set of first order initial value differential equations required to be solved for the stress state of Layer 2 at the end of its quenching phase. Similar to Eq. (14) these equations can be represented in matrix form, i.e.

$$D(T,\beta) = \begin{pmatrix} \dot{\beta}_1 \\ \dot{\beta}_2 \\ \dot{\beta}_3 \end{pmatrix} = \begin{bmatrix} 1 & -\nu_\ell & \frac{(2\beta_0-\beta_1)}{3Y(T)} \\ -\nu_\ell & 1 & \frac{(2\beta_1-\beta_0)}{3Y(T)} \\ \frac{(2\beta_0-\beta_1)}{Y(T)} & \frac{(2\beta_1-\beta_0)}{Y(T)} & 0 \end{bmatrix}^{-1} \begin{bmatrix} -E_\ell\alpha_\ell \\ E_\ell\alpha_\ell\left(\left(\frac{T_i-T_{q_2}}{T_p-T_{q_2}}\right) - 1\right) \\ 2\dot{Y} \end{bmatrix} \tag{28}$$

where β_0, β_1 and β_2 are respectively equal to $\sigma^{(q)}_{\ell_2(x)}$, $\sigma^{(q)}_{\ell_2(y)}$ and $E_\ell\lambda^{(q)}$, while D and Y bear their previous meanings.

As illustrated in Fig. 10, which shows extracts from temperature results at distinct stages during the thermal changes in the respective systems for the different deposition intervals, it is important to note from the figure that at the deposition of Layer 2 onto the composite S1, the latter is at some temperature, T_i, whose magnitude as already mentioned earlier depends on the time interval for the deposition of the former. With the assumption that the quenching of Layer 2 to the temperature T_{q_2}, is affected by the interfacial surface of the composite, implies Layer 1 is reheated from the temperature, T_i to the quenching temperature, T_{q_2}. This effect is

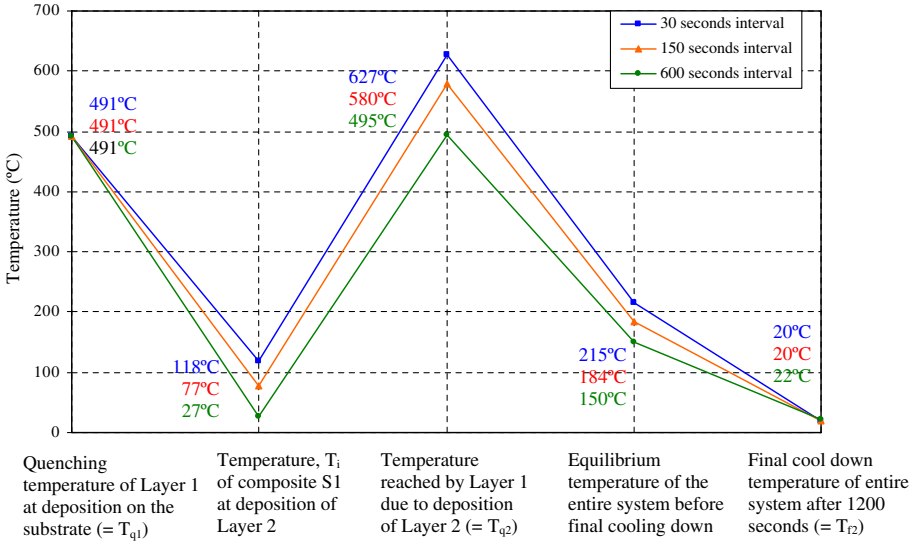

Fig. 10. Extracts from their respective thermal histories, showing temperatures in the Two-layer system at distinct periods starting from the deposition of Layer 2 to the final cool down state.

assumed to cause stress relaxation on Layer 1 from its initial pre-stressed state before the deposition of Layer 2.

It is also worth noting at this point that after the quenching of Layer 2, which is the commencement of the final cooling phase, the uniformity in material properties particularly the thermal expansion coefficients of Layer 1 and Layer 2 enhances their cohesion into a coating layer of thickness, $2h_\ell$, which cools down simultaneously with the substrate. Making the assumption that under such cohesion, the so-formed two-layer coating has uniform stress whose magnitude is the average of the stresses in the constituent layers at the end of the quenching phase requires knowledge of the respective stress states of the layers at that instant. Obviously, for Layer 2, its stress state at the end of its quenching phase are the values $\beta_0(T_{q_2})$, $\beta_1(T_{q_2})$ and $\beta_2(T_{q_2})$, which are obtained from the solution of the matrix in Eq. (28).

For Layer 1 its stress state is determined through the assumption that during its reheating from T_i to T_{q_2}, this layer and the substrate behave as a one-layer system at an initial temperature, T_i, at which the initial stress condition of the layer is $\beta_0(T_i)$, $\beta_1(T_i)$ and $\beta_2(T_i)$ whose values can be obtained by solving the matrix in Eq. (14) with a function, $S = \mathrm{Rkadapt}(Y0, T_{q_2}, T_i, N, D)$. Also, for the reheating of Layer 1, its material behaviour is tested for potential yielding using the condition

$$(\sigma_{(x)_i} + \Delta\sigma_{(x)})^2 + (\sigma_{(y)_i} + \Delta\sigma_{(y)})^2 \leqslant (Y_i)^2 \tag{29}$$

where $\sigma_{(x)_i}$ and $\sigma_{(y)_i}$ are stresses due to yielding and are obtained from Eq. (14) and $\Delta\sigma_x$ and $\Delta\sigma_y$ are incremental elastic stresses due to a temperature increment, ΔT.

When applied in the analysis of any process phase, satisfaction of the inequality in Eq. (29) confirms elastic deformation. Application of this equation confirmed elastic behaviour for the reheating of Layer 1. The corresponding equation to Eq. (12) for the reheating of Layer 1 is then not applicable; and those for Eqs. (10) and (11), respectively, take the forms

$$\dot{\sigma}^{(r)}_{\ell_1(x)} - \nu_\ell \dot{\sigma}^{(r)}_{\ell_r(y)} = -E_\ell \alpha_\ell \tag{30}$$

$$\dot{\sigma}^{(r)}_{\ell_1(y)} - \nu_\ell \dot{\sigma}^{(r)}_{\ell_1(x)} = E_\ell(\alpha_s - \alpha_\ell) \tag{31}$$

These equations in the matrix form are

$$D(T,\beta) = \begin{pmatrix} \dot{\beta}_0 \\ \dot{\beta}_1 \end{pmatrix} = \begin{bmatrix} 1 & -\nu_\ell \\ -\nu_\ell & 1 \end{bmatrix}^{-1} \begin{pmatrix} -E_\ell \alpha_\ell \\ E_\ell(\alpha_s - \alpha_\ell) \end{pmatrix} \tag{32}$$

The reheating of Layer 1 unifies its temperature and that of Layer 2 to T_{q_2}. At this uniform temperature from which both layers cool down as a combined layer of thickness, $2h_\ell$ to some final temperature T_{f_2}, the initial stress state of the combined layers has been assumed to be equal to the average of the stress state of Layer 2 at the end of its quenching process and that of Layer 1 at the end of its reheating process. For Layer 2, this stress state is as obtained from the solution of the matrix in Eq. (28), while for Layer 1, it is obtained from the solution of the matrix in Eq. (32).

During the final cooling phase, in which the so-formed two-layer coating behaves elastically, the process is definable by a matrix of the form in Eq. (20), which in this case is

$$D(T,\beta) = \begin{bmatrix} 1 & -\nu \\ -\nu & \left\{1 - \left(\frac{h_s}{2} - \omega_N\right)\phi_2 E_\ell\right\} \end{bmatrix}^{-1} \begin{bmatrix} -E_\ell \alpha_\ell \\ E_\ell(\alpha_s - \alpha_\ell) \end{bmatrix} \tag{33}$$

where all symbols bear their usual meanings; and ω_N, the position of the neutral axis of the two-layer system from the centroidal axis of the substrate is as defined in Eq. (A7) in Appendix A; and ϕ_2 is a parameter deduced from Eq. (A9) in the same appendix as $\phi_2 = -12bh_\ell(h_s + 2h_\ell - 2\omega_N)/E_s(bh_s^3 + 12bh_s\omega_N^2)$.

From the solution of vectors $\beta_0(T_{2\ell})$ and $\beta_1(T_{2\ell})$, the value of $\beta_1(T_{f_2})$ represents the in-plane stress, $\sigma^{(f)}_{2\ell(y)}$. This is the residual stress in the two-layer coating, which for convenience is identified as $\Delta\sigma_{2\ell}$, which represents the stress change in the so-formed two-layer coating from its stress-free state to its final cool down state.

To calculate the residual stress, $\Delta\sigma_{2\ell}$ in a two-layer system, information about the temperatures, T_{q_1}, T_i, T_{q_2} and T_{f_2} is required. For the deposition intervals of 30, 150 and 600 s, which are studied between the depositions of Layer 1 and Layer 2, the values of these temperatures as estimated from the thermal results of the

finite element models are as illustrated in Fig. 10. Appropriate substitution of these temperatures into either the matrices defined by Eqs. (28), (32) and (33) or their solution functions gives the residual stress, $\Delta\sigma_{2\ell}$, in a two-layer coating. Respective substitution of this stress for the different deposition intervals into a combination of Eq. (1) and Eqs. (A7), (A8) and (A9) in Appendix A gives the corresponding values of the average interfacial residual stress in the so-formed two-layer coating systems from the different deposition intervals. A plot of the variation of this average interfacial stress with layer deposition interval is included in Fig. 5.

For the simplified numerical modelling investigation on the effect the number of layers in a coating, the average interfacial residual stress in the two systems was deduced following the same approach used in the experimental investigation. Similar to the results from the experimental investigation, these stresses as presented in Fig. 6 also have opposite signs.

4. Finite element modelling

Residual stress in thermally sprayed coatings is generated through the rapid solidification and eventual cooling of molten droplets impinging and spreading on a substrate or previously deposited layer. Using the finite element method, modelling its state in coated systems therefore requires a thermo-structural analysis, suitably with the Direct method due to the nonlinearities involved from phase change and elastic-plastic deformation. With the involvement of such phenomena, accurate modelling of the physics requires the solution of a highly nonlinear problem, where the numerical algorithms can adversely affect the results. Considering the potential difficulty in formulating a model for such process, particularly if all the process parameters are to be taken into account, the following assumptions have been utilised to simplify the analysis using the Ansys software.

(a) The droplet deposition process involves impact and spreading. Since this is completed over a time scale much shorter than the time needed for the droplet to solidify the initial spreading process can be justifiably neglected (Amon et al., 1994, 1996; Trapaga et al., 1992; Fukai et al., 1993; Clyne, 1984). This assumption uncouples the problem from the fluid dynamics and simplifies it to just heat transfer and structural mechanics.
(b) All droplets in a layer are at uniform initial temperature and each layer is assumed to constitute all droplets of spray passes at the same horizontal level.
(c) For coatings with more than one layer, a current layer is modelled in the liquid state from which it solidifies. The substrate and all previously deposited layers are modelled in the solid state.
(d) Part of a coating process is the application of a bond-coat on the substrate before applying the top coating. But due to the much thinner nature of this bond-coat compared to the layers of the top-coat, and its similarity in this research to the substrate material in terms of both being copper-based alloys, the bond-coat is assumed to be integrated within the thickness of the substrate.
(e) The coating and substrate are in very good contact and as assumed elsewhere (Passandideh-Fard et al., 1999) a constant heat transfer coefficient of 10^7 W/m^2 °C is introduced at the interface between the layers, and between the coating and the substrate to simulate such contact between the surfaces.
(f) All materials are generally assumed isotropic. Specifically, the substrate is assumed elastic while all coating layers which are assumed to undergo yielding are assumed elastic-perfectly plastic.

Following these assumptions, Fig. 11 was developed as a sufficient geometrical representation of the problem under investigation, including one-half of its physical layout due to symmetry about mid-length in the *xz*-plane; and basically presenting the situation of a one-layer coating on the substrate.

For this type of analysis with Ansys, the geometry was meshed with PLANE13 element. This element type supports both plane strain and plane stress formulations, which serve as approximations to the 3-D stress system generated during the cooling of a layer. However, in the 2-D models, a plane strain approximation has been used for the different coating/substrate systems. The rational behind this approximation is based on the fact that during the quenching phase in the cooling of a layer, the layer is evidently in plane strain. In addition to this, consideration is given also to the coating of surfaces in practice. This is done on large surfaces in which plane strain assumption is more appropriate. These factors are viewed as simple justifications for the use

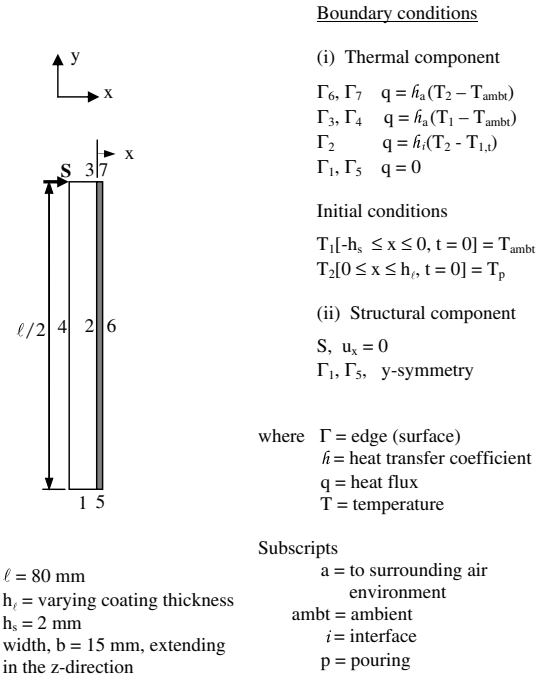

Fig. 11. Two-dimensional model, showing geometry and boundary conditions.

of this element with plane-strain assumptions in the different models. In addition to the use of this element for the physical domains of the geometry, note was also taken of the interfacial contact between the coating and the substrate as well as that between coating layers. Assuming such contacts to be surface-to-surface, contact elements were used at all interfaces. CONTA171, a 2-D surface-to-surface contact element was specifically used based on its nodal compatibility with the underlying PLANE13 element.

In establishing mesh convergence, a 0.1 mm coating layer was modeled on the 2 mm substrate and four meshes, called Mesh 0, Mesh 1, Mesh 2 and Mesh 3 were tried. The focus of the convergence study is on the value of the stress on the coating at the interface since this is critical to the performance of the coating layer. The respective values of this stress for the four trial meshes are −72.3, −76.1, −77.7 and −78.6 MPa. Recognising the practical limitations in the accuracy achievable for this process, Mesh 1 was considered to be sufficiently accurate for the analysis. This mesh is such that the substrate, which is always 2 mm thick, has a density of 2400 elements and for the coating, which depending on the thickness investigated has 1200 elements for every 0.1 mm thickness.

The boundary conditions, which define the modes of heat transfer, structural loading and constraints on the different parts of the system, are as defined in Fig. 1. Based on the assumption of very nearly perfect (bonded) contact between coating layers as well as between coating and substrate, a constant heat transfer coefficient, h_i of 10^7 W/m^2 °C was used at all interfaces within a coating/substrate system. Also, for models involving more than one coating layer the element birth and death feature was used to simulate the addition of a current and stress-free layer onto an initially stressed system.

With regards to material properties, the physical geometry of the coating/substrate assembly should ideally constitute a substrate of chrome copper (Cu 99.1, Fe 0.01, Cr 0.60, Si 0.10, Mn 0.05), a bond-coat of Tafa Arc Spray Aluminium Bronze 10 T (Cu 92.25, Al 7.0, Fe 0.5) and a top-coat of Tafa 95 MXC Ultra Hard Armacorn wire of chromium steel (Si 1.6, Cr 29.0, Mn 1.65, B 3.75, Fe 64). However, as mentioned above the bond-coat being integrated into the thickness of the substrate simplified the material constitution within the models to two materials, i.e. those of the substrate and the top-coat only. Since the analysis is thermo-structural, both thermal and structural physical properties are required.

For the thermal properties, currently deposited layers, which undergo solidification and then gradual cooling, temperature-dependent material property data is required, i.e. thermal conductivity $k(T)$ and enthalpy, $H(T)$. For the copper substrate, and all previously deposited layers, which are assumed to have solidified, temperature-independent properties are used and these are the thermal conductivity, k; density ρ; and specific heat c_p.

Based also on the assumption that all materials are isotropic the structural component of the material properties needed includes the thermal expansion, α; density, ρ; Young's modulus, E; Poissons ratio; v and the yield stress, Y. Also, since a deposited layer is initially at a stress-free temperature and gradually become stressed and deformed due to temperature change, the specification of temperature-dependent yield stress, $Y(T)$ was considered appropriate with a zero tangent modulus at all temperatures based on the assumption that the coating material is elastic-perfectly plastic. A summary of the specific physical property values used for each of the materials and values of heat transfer coefficients used in the models is presented in Table 1. The value of E chosen in Table 1 is below that typical for high-chromium steels to reflect the presence of porosity (≈10%). Young's Modulus can vary significantly with temperature but for the reasons of model simplicity and absence of published information, an invariant value was used.

4.1. Finite element modelling results

4.1.1. Deposited layer thickness

Fig. 12 shows comparative plots for the through-thickness stress distribution in the three achievable one-layer coating systems over a period of 600 s. For all layers, the figure indicates a compressive residual stress (with highest effect at the interface) in the coating, a tensile stress at the interface on the substrate and a compressive stress at the rear of the substrate. With the thermal expansion coefficient of the coating being smaller than that of the substrate (i.e. $\alpha_\ell < \alpha_s$) such distribution pattern for the residual stress in the one-layer coating systems indeed agrees with both the prediction by (Pawlowski, 1995) on the nature of residual stress in a thermally sprayed coating layer, and the experimental works referenced by (Takeuchi et al., 1990) to confirm that prediction. The result also suggests that for each of the layers the compressive stress generated (due to shrinkage) during final cooling dominated the tensile stress from quenching. As defined in Eq. (1), the average

Table 1
The specific material property values and heat transfer coefficients used in the thermo-structural analysis

PROPERTY		PART OF MODEL AND MATERIAL							
		Substrate (Copper)	Coating[a] (Steel)						
			Currently deposited layer						Previously deposited layer
Density (kg/m^3)	ρ	8410	7850						
Specific heat capacity (J/kg)	c_p	473							450
Enthalpy x 10^9 (J/m^3)	H		T	0	1425	1489	1607		
			H	0	7.09	9.46	10.0		
Thermal conductivity (W/m^{O}C)	k	334	T	0	795.2	1419	1476.2	1600	
			k	60	25.79	31.58	43.25	43.25	42
Heat transfer coefficient (W/m^{2}K)	h_a	20							
	h_i	10^7							
Young's Modulus (GPa)	E	110	200						
Poisson's Ratio	ν	0.35	0.25						
Yield Stress (MPa)	Y	122	T	20	472	827	1227	1727	
			σ_y	280	155	82	10	0	
Thermal expansivity (10^{-6}/^{O}C)	α	17	11.3						

Note. T, represents temperature (°C).

[a] Assumed to be 304L stainless steel for which temperature-dependent enthalpy and thermal conductivity were obtained from Thomas et al. (1987), the temperature-dependent yield stress adopted from Ortega et al. (1998) and others from Brandes (1993) and ASM Intl. (1990).

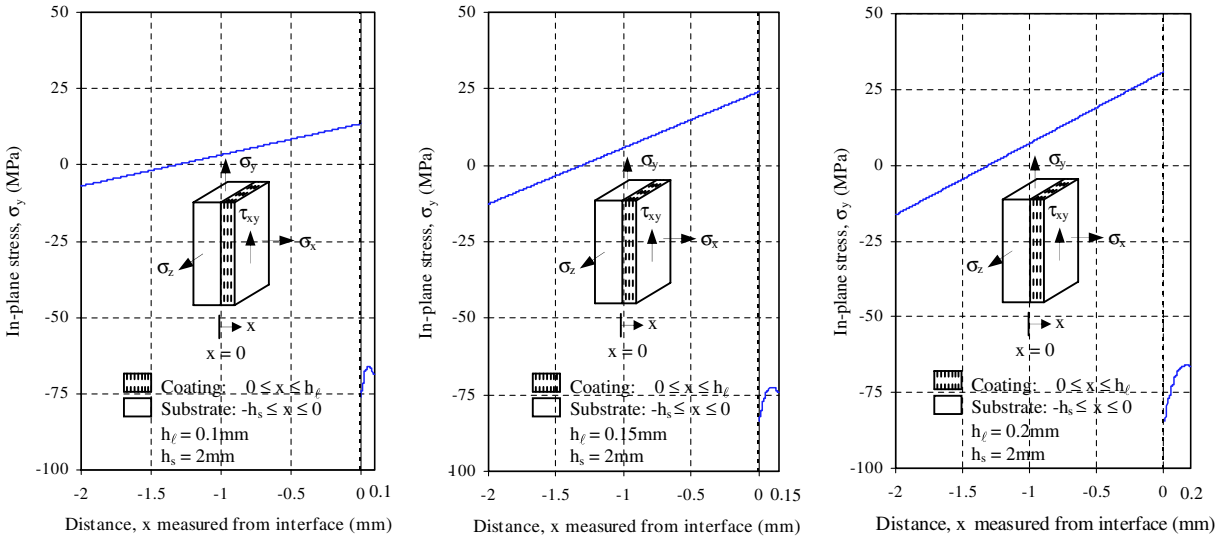

Fig. 12. Residual stress distribution in the 0.1, 0.15 and 0.2 mm coating systems.

interfacial residual stress is calculated for the respective plots and its variation with deposited layer thickness is included in Fig. 3.

4.1.2. Interval of layer deposition

Resulting from the deposition intervals of 30, 150 and 600 s, which were respectively modelled between the depositions of Layer 1 and Layer 2 are the plots in Fig. 13, which for the respective cases of deposition inter-

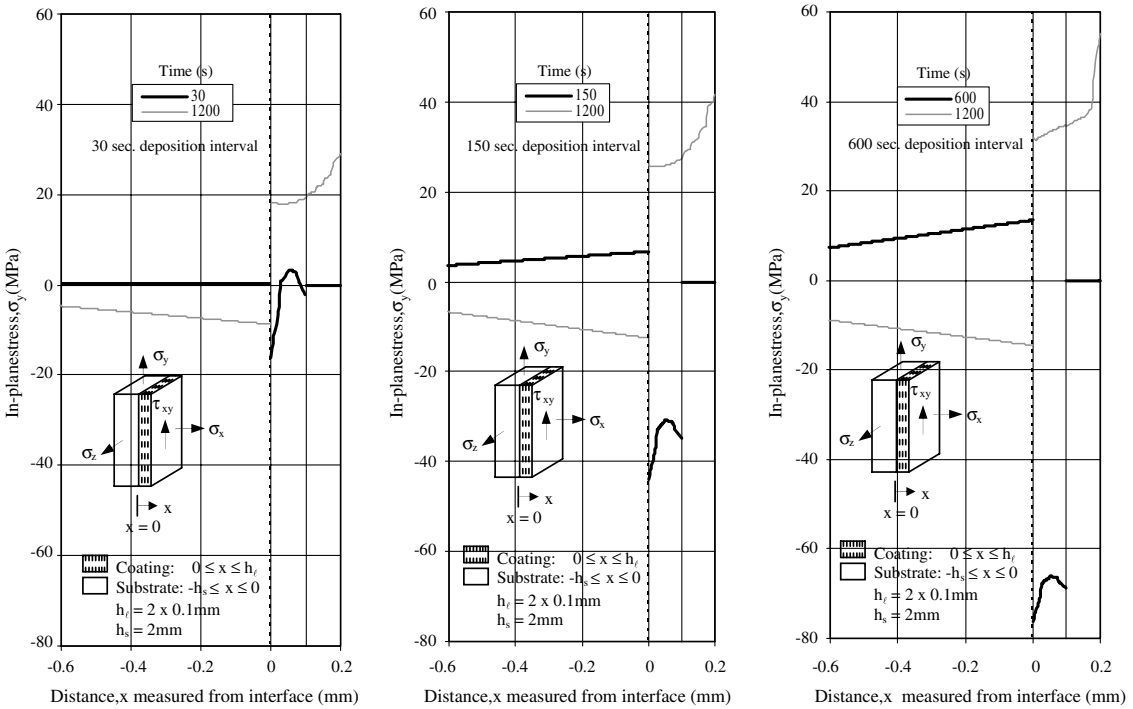

Fig. 13. Residual stress distribution in the so-formed two layer coating systems and a depiction of the change in the direction of the stress in the system due to the deposition of Layer 2.

vals show the through-thickness stress distribution in the entire coating/substrate system, at the end of 1200 s after the deposition of Layer 1. From the plots, it is interesting to note the change in the direction of the stress in each system due to the deposition of Layer 2. Such change could be attributed to the relative values of the coefficients of thermal expansion, which as mentioned elsewhere (Liu and Murarka, 1992) determines the sign of the stress in each layer of a coated system. Furthermore, an explanation to the effect considered the thermal behaviour of the entire system during both the quenching and final cooling of Layer 2. Due to quenching, Layer 2 acquires tensile stress from its resisted contraction by its interfacial cohesion onto Layer 1. The quenching of Layer 2 gives rise to temperature rise in the underlying Layer 1/substrate couple to some common bulk temperature with Layer 2. In the simply-supported system, Layer 1/substrate couple is free to expand but restrained only at its interfacial surface with Layer 2. Since for the Layer 1/substrate couple $\alpha_s > \alpha_\ell$, the enhanced expansion of Layer 1 and the retarded expansion of the substrate will result in a tensile stress set-up in Layer 1 and a predominant compressive stress in the substrate. During final cooling down of the entire system from the common bulk temperature which they attained to possibly room temperature, the two layers are assumed to have cohered to each other as a single coating layer on the substrate. Here also, since $\alpha_s > \alpha_\ell$ the enhanced contraction of the coating layer and retarded contraction of the substrate generates compressive stress in the coating and a predominant tensile stresses in the substrate. However the resultant tensile and compressive stress, which resulted in the coating and the substrate respectively, indicate that the stress from quenching dominated that from final cooling down. Estimated from the plots in Fig. 13 are the respective average interfacial stresses. The variation of this stress with layer deposition interval is included in Fig. 5.

4.1.3. Number of layers in a coating

Maintaining the approach used in the experimental and the simplified numerical modelling investigations, information for the average interfacial stress in the one-layer and the two-layer coating systems with the finite element method was deduced as presented in Fig. 6. As with the corresponding results from the two other investigation methods, this results maintain an opposing sign in the stresses in the two systems.

5. Discussion of results

Presented in Fig. 3 are plots showing the variations of the average interfacial stress with deposited layer thickness for the three investigation methods considered. Similar plots for the variations of the average interfacial stress with interval of layer deposition are presented in Fig. 5. In Fig. 3, appreciable agreement between the finite element modelling and the simplified numerical modelling results is seen for smaller layer thicknesses such as 0.1 mm. The agreement in the two results is seen to diminish rapidly with increase in layer thickness. In Fig. 5, the agreement between the finite element and the simplified numerical modelling results is seen to be fairly good. This can be attributed to the small layer thickness involved, which is 0.1 mm for each of the two sequentially deposited layers that were considered in the investigations on the effect of layer deposition interval on stress. However, whatever level of disagreement observed between the two results could be due to the use of node-based temperature estimates from the finite element results, which were used for the stress calculations in the simplified numerical analysis. The use of these unified temperatures may not be sufficient since thermal gradients are present in the thermal spraying process.

Relative to both the experimental and the simplified numerical modelling results, the results from the finite element modelling are seen in both Figs. 3 and 5 to be over-predicting. Among possible causes for this is the temperature of 1600 °C, which is assumed in the finite element analysis as initial temperature for a layer. Irrespective of the magnitude of the temperature with which a coating leaves a spray gun, its loss during flight causes it to be at much lower value by the time it contacts the substrate. Secondly, a coating layer is in practice deposited on a substrate at smaller droplets with energy release during solidification and cooling, which contributes to the generation of stress. In the finite element analysis, all particles in a layer of coating are assumed as a single block. The energy release from such block, which is assumed to be initially at 1600 °C can therefore be comparatively higher with corresponding higher stress levels as observed.

However, irrespective of the identified disagreement in stress magnitudes, it generally suffices to say that the plots in Fig. 3 agreeably indicate a compressive average interfacial stress in the one-layer coating systems stud-

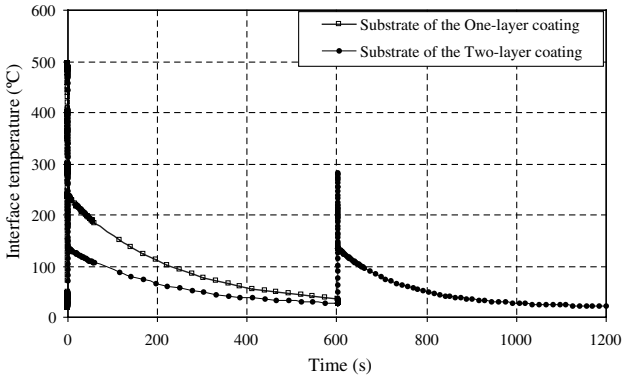

Fig. 14. Interfacial temperature history of the substrates for the One-layer and the Two-layer coatings, showing their heating patterns.

ied; and that this stress changes progressively from compressive towards tensile with increase in deposited layer thickness. Noting therefore that debonding is associated with coatings in which the tensile stress in the bond line (i.e. the interface) is high (often in excess of the bond strength or cohesive strength), the results then generally suggests an increase in the potential for debonding with increase in deposited layer thickness. In Fig. 5, similar agreement of a tensile average interfacial stress is seen in the two-layer coating systems formed from the different deposition intervals. This stress, which is also seen to increase progressively in the tensile direction with increase in interval of layer deposition also suggests an increase in the potential for coating debonding with increase in the interval of layer deposition.

With regard to the investigation on the number of layers in a coating, Fig. 6 indicates for each investigation method that the average interfacial stresses in the one-layer and the two-layer coatings are in opposite directions. With such opposing stress directions, a stress-based comparison on the relative influence of the stress in the two systems towards coating performance is difficult. Focus was therefore made on the thermal behaviour of the substrates of the two systems as presented in Fig. 14, which shows respectively, their interface temperature histories. It can be deduced from the figure that the interface on the one-layer system attained higher temperature with delayed cooling compared to that on the two-layer system. Of course, high substrate interfacial temperatures in coating systems are only advantageous if they could effect interface melting, which promotes interfacial bonding in the system. Otherwise, high interfacial temperatures with delayed cooling as observed from the one-layer system compared to the two-layer system basically enhances interfacial oxidation. This effect often causes the formation of an oxide layer at the interface which weakens the bond. The higher interfacial temperature in the one-layer coating system therefore suggest higher potential to the formation of an oxide layer at the interface, which consequently implies higher potential to coating debonding compared to the two-layer system.

6. Conclusions

The different investigation methods have studied the effects of deposited layer thickness, interval of layer deposition and number of layers in a deposited coating for their effects on the nature of the residual stress and the trend of its change with increase in coating thickness. The main focus has been on the influence of these layer deposition options on the performance of steel coating and more importantly their bonding onto a copper substrate. The results from the different methods of investigations agreeably revealed the following conclusions:

- For block deposition, (i.e. the deposition of a required thickness of coating as a single layer), the thicker the layer the higher the potential for debonding.
- A thick coating deposited as block has a higher potential to debond compared to the same thick coating deposited in multiple thinner layers.
- In the deposition of multiple layers the longer the interval of deposition between the layers the higher the potential for the coating to debond. This observation is a possible justification for why progressive layer deposition is adopted in most thermal spray practices.

On the whole, a reasonable suggestion from the above observations is that the development of thick and well bonded coatings could be enhanced through deposition of thinner layers at very short intervals or even progressively.

Appendix A

A.1. Curvature change in one-layer and two-layer coating systems

A.1.1. One-layer system

Shown in Fig. A.1 is a tensile stress change, $\Delta\sigma_\ell$, defining the residual stress in the layer. The resulting incremental force, ΔF_ℓ set up in the layer is $\Delta F_\ell = bh_\ell\Delta\sigma_\ell$, which gives rise to an incremental moment ΔM_ℓ and both of which are balanced through curvature adoption by the composite system. It is assumed here, as a consequence of the comparatively thin coating layer compared with the substrate ($h_\ell \ll h_s$), that bending of the composite is dictated by the elastic behaviour of the substrate. As shown in the figure, the resulting stress set up in the substrate is of form

$$\Delta\sigma_s = \frac{-\Delta F_\ell}{bh_s} + \frac{\Delta M_s}{I_s} w \tag{A1}$$

where I_s is the second moment of area of the substrate about y_s–y_s and ΔM_s is the positive bending moment on the substrate about the same axis. But $\Delta M_s = -\Delta M_\ell$, where ΔM_ℓ, the incremental moment of the force, ΔF_ℓ about $y_s - y_s$ is $\Delta M_\ell = \Delta F_\ell(h_s + h_\ell)/2$

At the neutral axis the incremental stress is zero, obtaining from (A1) the position, w_N of the neutral axis, N–N measured from the axis, y_s–y_s as

$$w_N = -\frac{h_s^2}{6(h_s + h_\ell)} \tag{A2}$$

From the approximation of a coated system to a thin beam the residual stress at the interfacial surface of a coated substrate is

$$\Delta\sigma_s|_{x=0} = E_s\left(\frac{h_s}{2} - w_N\right)\Delta\kappa \tag{A3}$$

and the flexure formula, which is thus applicable means the curvature change in the system, which is dictated by the elastic behaviour of the substrate is $\Delta\kappa = \Delta M_s^*/E_s I_s^*$, where the ΔM_s^* and I_s^* are incremental moment in the substrate and second moment of area of the substrate about the neutral axis, N–N. As derived from Fig. A.1 a substitution for these parameter into the equation gives

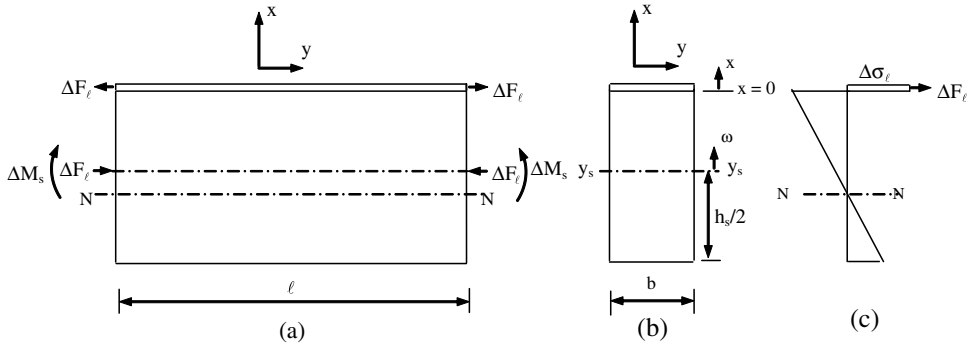

Fig. A.1. Schematic illustration of the induced forces and moments due to an assumed tensile residual stress, $\Delta\sigma_\ell$, generated in the coating of a one-layer system and the resulting stress profile in the layer/substrate system.

$$\Delta\kappa = -\frac{6bh_\ell(h_s + h_\ell - 2w_N])\Delta\sigma_\ell}{E_s(bh_s^3 + 12bh_s w_N^2)} = \phi\Delta\sigma_\ell \tag{A4}$$

A.1.2. Two-layer system

For the two-layer system depicted in Fig. A.2, the assumed uniform stress change, $\Delta\sigma_{2\ell}$, sets up a force change, $\Delta F_{2\ell}$ in the layer; and of magnitude $\Delta F_{2\ell} = 2bh_\ell\Delta\sigma_{2\ell}$, which gives rise to a moment change, $\Delta M_{2\ell}$. Similar to Eq. (A1) the resulting stress profile in the substrate of the two-layers is

$$\Delta\sigma_{2\ell} = \frac{\Delta F_{2\ell}}{bh_s} + \frac{\Delta M_s}{I_s}\omega \tag{A5}$$

Moment equilibrium in the system gives $\Delta M_s = -\Delta M_{2\ell}$, where $\Delta M_{2\ell}$ is the moment generated by the force, $\Delta F_{2\ell}$ about y_s–y_s and is defined by $\Delta M_{2\ell} = \Delta F_{2\ell}(h_s + 2h_\ell)/2$. Substituting for I_s and ΔM_s into Eq. (A5) and noting that the stress is zero at the neutral axis gives the position, ω_N of the neutral axis of the two-layer system from the axis, y_s–y_s as

$$\omega_N = -\frac{h_s^2}{6(h_s + 2h_\ell)} \tag{A6}$$

Defining $\bar{h} = h_\ell/h_s$ this is further simplified to

$$\omega_N = -\frac{h_s^2}{6(h_s + h_\ell)}\left(\frac{1+\bar{h}}{1+2\bar{h}}\right) = \left(\frac{1+\bar{h}}{1+2\bar{h}}\right)w_N \tag{A7}$$

Following similar arguments involved in the derivations for the one-layer system, the stress change at the interfacial surface of the substrate of the two-layer coating is

$$\Delta\sigma_s|_{x=0} = E_s\left\{\frac{h_s}{2} - \left(\frac{1+\bar{h}}{1+2\bar{h}}\right)w_N\right\}\Delta\kappa \tag{A8}$$

and the change in curvature is

$$\Delta\kappa = -\frac{12bh_\ell(h_s + 2h_\ell - 2\omega_N)\Delta\sigma_{2\ell}}{E_s(bh_s^3 + 12bh_s\omega_N^2)} = \phi_2\Delta\sigma_{2\ell} \tag{A9}$$

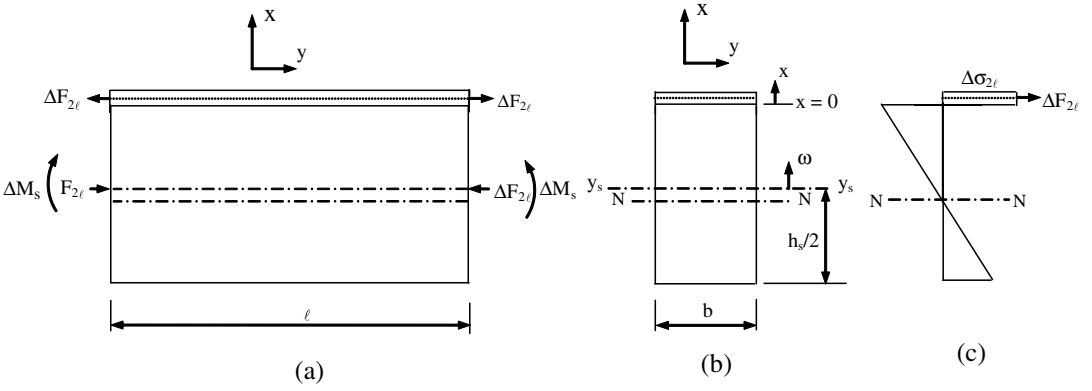

Fig. A.2. Schematic illustration of the induced forces and moments due to an assumed tensile residual stress, $\Delta\sigma_{2\ell}$, generated in the coating of a two-layer system and the resulting stress profile in the coating/substrate system.

Appendix B

B.1. MathCAD's adaptive Runge-Kutta function (Rkadapt)

The function Rkadapt refers to an adaptive Runge-Kutta ordinary differential equation numerical solver used in the mathematical software package, MathCad. Its application as used with the simplified numerical models is illustrated in this appendix by considering a coating layer undergoing a phase of temperature change from an initial value of T_1 to some final value of T_2. The resulting stress state in the principal directions of the layer, which are a function of the layer temperature, T_ℓ are considered to be of the form defined by Eqs. (10)–(12). Written in the matrix form, these equations take the form in Eq. (14), whose solution is obtained with an adaptive Runge-Kutta function of the form

$$S = \mathrm{Rkadapt}(Y0, T_1, T_2, N, D) \tag{B1}$$

where D and N bear their previous meanings, and T_1 and T_2 are the initial and final temperatures of the process phase concerned. $Y0$ is the vector of initial conditions, $\beta_0(T_1)$, $\beta_1(T_1)$ and $\beta_2(T_1)$, defining the stress state of the layer at the initial temperature, T_1. This is of the form

$$Y0 = \begin{bmatrix} \beta_0(T_1) \\ \beta_1(T_1) \\ \beta_2(T_1) \end{bmatrix} \tag{B2}$$

S is the matrix of the solution vectors for $\beta_0(T_\ell)$, $\beta_1(T_\ell)$ and $\beta_2(T_\ell)$, at the N solution points from T_1 to T_2, from which the stress condition of the layer at the temperature T_2 is identified by $\beta_0(T_2)$, $\beta_1(T_2)$ and $\beta_2(T_2)$.

References

Ahmed, R., Hadfield, M., 1997. Experimental measurement of the residual stress field within thermally sprayed rolling elements. Wear 209, 84–95.

Amon, C.H., Merz, R., Prinz, F.B., Schmaltz, K.S., 1994. Thermal modelling and experimental testing of MD spray shape deposition processes. In: Heat transfer, Proceedings of 10th International Heat Transfer Conference, vol. 7, Brighton, UK, pp. 321–324.

Amon, C.H., Merz, R., Prinz, F.B., Schmaltz, K.S., 1996. Numerical and experimental investigation of interface bonding via substrate melting of an impinging molten metal droplet. Journal of Heat Transfer 118, 164–172.

Araujo, P., Chicot, D., Staia, M., Lesage, J., 2005. Residual stresses and adhesion of thermal spray coatings. Surface Engineering 21 (1), 35–40.

ASM Intl., Metals Park, 1990. Metals Handbook, 10th ed., vol. 2.

Borland, D.W., 1994. Residual Stress Measurement – Methods, Limitations and Significance. In: Proceedings of the Second Australian International Conference on Surface Engineering Coatings and Surface Treatments in Manufacturing; Adelaide, South Australia; Australia, pp. 114–121.

Brandes, E.A., 1993. Smithells Metals Reference Hand Book, 6th ed. Butterworths, United Kingdom.

Clarke, L.D., Alonso Rasgado, M.T., Davey, K., Hinduja, S., 2006. Experimental investigation into the thermal behaviour of copper-alloyed dies in pressure die casting. Trans. ASME, Journal of Manufacturing 128, 844–859.

Clyne, T., 1984. Numerical treatment of rapid solidification. Metallugical and Materials Transactions B 15B, 369–381.

Clyne, T.W., Gill, S.C., 1996. Residual stresses in thermal spray coatings and their interfacial adhesion: a review of recent work. Journal of Thermal Spray Technology 5 (4), 401–418.

Fukai, J., Zhao, A., Poulikakos, D., Megaridis, C.M., Miyatake, O., 1993. Modelling of the deformation of a liquid droplet impinging upon a flat surface''. Physics of Fluids A 5, 2588–2599.

Gill, S.C., Clyne, T.W., 1994. Investigation of residual stress generation during thermal spraying by continuous curvature measurement. Thin Solid Films 250, 172–180.

Godoy, C., Souza, E.A., Lima, M.M., Batista, J.C.A., 2002. Correlation between residual stresses and adhesion of plasma sprayed coatings: effects of post-annealing treatment. Thin Solid Films, 420–421, 438-445.

Kesler, O., Matejicek, J., Sampath, S., Gnaeupel-Herold, T., Brand, P.C., Prask, H.J., 1998. Measurement of residual stress in plasma-sprayed metallic, ceramic and composite coatings. Materials Science and Engineering A257, 215–224.

Knight. R., Smith, R.W., 1993. Residual stress in thermally sprayed coatings. In: Proceedings of National Thermal Spray Conference, Anaheim, pp. 607–612.

Kuroda, S., Clyne, T.W., 1991. The quenching stress in thermally sprayed coatings. Thin Solid Films 200, 49–66.

Larsson, M., Hedenqvist, P., Hogmark, S., 1996. Deflection measurements as a method to determine residual stress in thin hard coatings on tool materials. Surface Engineering 12 (1), 43–48.

Liu, H.C., Murarka, S.P., 1992. Elastic and viscoelastic analysis of stress in thin films. Journal of Applied Physics 72 (8), 3458–3463.

Lugscheider, E., Nickel, R., 2003. Finite element Simulation of a Coating Formation on a Turbine Blade during Plasma Spraying. Surface and Coatings Technology, 174–175, 475-481.

Noyan, I.C., 1992. Defining residual stresses in thin film structures. Advances in X-ray Analysis 35A, 461–473.

Ortega, A.R., Dike, J.J., Lathro, J.F., Cadden, C.H., Folk, D.R., Robles, J.E., 1998. Analysis and validation of multi-pass girth welds in pipes. In: Proceedings of 8th International Conference on Modelling of Casting and Welding Processes, San Diego, California.

Passandideh-Fard, M., Mostaghim, J., Chandra, S., 1999. Modelling sequential impact of two molten droplets on a solid surface. In: The ILASS-Americas 12th Annual Conference on Liquid Atomisation and Spray Systems, Indianapolis, IN.

Pawlowski, L., 1995. The Science and Engineering of Thermal Spray Coatings. Wiley and Sons, London.

Perry, J.A., Sue, J.A., Martin, P.J., 1996. Practical measurement of the residual stress in coatings. Surface and Coatings Technology 81, 17–28.

Takeuchi, S., Ito, M., Takeda, K., 1990. Modelling of residual stress in plasma-sprayed coatings: effect of substrate temperature. Surface and Coatings Technology (43/44), 426–435.

Thomas, B.G., Samarasekera, I.V., Brimacombe, J.K., 1987. Mechanical model of the thermal processing of steel ingots: Part I. Heat flow mode. Metallurgical Transactions B, 119–129.

Totemeire, T.C., Wright, J.K., 2006. Residual stress determination in thermally sprayed coatings – a comparison of curvature models and X-ray techniques. Surface and Coatings Technology 200, 3955–3962.

Trapaga, G., Matthys, E.F., Valencia, J.J., Szekeley, J., 1992. Fluid Flow, heat transfer and solidification of molten droplets impinging on substrates: comparison of numerical and experimental results. Metallurgical and Materials Transactions B 23B, 701–718.

Tsui, Y.C., Clyne, T.W., 1997a. An analytical model for predicting residual stresses in progressively deposited coatings, Part 1: planar geometry, 1997. Thin Solid Films 306, 23–33.

Tsui, Y.C., Clyne, T.W., 1997b. An analytical model for predicting residual stresses in progressively deposited coatings, Part 2: cylindrical geometry. Thin Solid Films 306, 34–51.

Vijgoen, R.O.E., Dautzenberg, J.H., 1995. Mechanical measurement of the residual stress in thin PVD films. Thin Solid Films 270, 264–269.

Withers, P.J., Bhadeshia, H.K.D.H., 2001. Residual Stress – I: Measurement Techniques. Materials Science and Technology 17, 355–365.